Clim Dyn (2016) 47:2747–2764
DOI 10.1007/s00382-016-2995-9

Diagnosing the possible dynamics controlling Sahel precipitation in the short-range ensemble community atmospheric model hindcasts

Yu-heng Tseng[1] · Yen-heng Lin[2] · Min-hui Lo[2] · Shu-chih Yang[3]

Received: 4 September 2015 / Accepted: 15 January 2016 / Published online: 27 January 2016

Abstract The actual dynamics and physical mechanisms affecting the Sahel precipitation pattern and amplitude in the climate models remain under debate due to the inconsistent drying and rainfall variability/pattern among them. We diagnose the boreal summer rainfall pattern in the Sahel and its possible causes using short-range ensemble hindcasts based on NCAR community atmospheric model with the local ensemble transform Kalman filter (CAM-LETKF) data assimilation. The CAM-LETKF assimilation was conducted using 64 ensemble members with an assimilation cycle of 6-h. By comparing the superior and inferior groups within these 64 ensembles, we confirmed the influence of the Atlantic in the West Sahel rainfall (a robust feature in the ensembles) and a severe model bias resulting from erroneously modeled locations and magnitudes of low-level Sahara heat low (SHL) and African easterly jet (AEJ). This bias is highly related to atmospheric jet dynamics as shown in recent studies and local wave instability triggered mainly by the boundary-layer temperature gradient and amplified by land–atmosphere interactions. In particular, our results demonstrated that more accurate divergence and convergence fields resulting from improved SHL and AEJ in the superior groups enabled more accurate rainbelt patterns to be discerned, thus improving the ensemble mean model hindcast prediction by more than 25 % in precipitation and 16 % in temperature. We concluded that the use of low-resolution climate models to project future rainfall in the Sahel requires caution because the model hindcasts may quickly diverge even the same boundary conditions and forcings are applied. The model bias may easily grow up within a few months in the short-range CAM-LETKF hindcast, let along the free model centennial simulations. Unconstrained future climate model projections for the Sahel must more effectively capture the short-term key boundary-layer dynamics in the boreal summer to be credible regardless model dynamics and physics.

Keywords Land–atmosphere interaction · Global climate model evaluation · Sahel precipitation · Local ensemble transform Kalman filter (LETKF) · Model uncertainty

1 Introduction

Studies have extensively documented that the Sahel—the transitional zone between the Sahara Desert and the rainforests of Central Africa and the Guinea Coast—has experienced a severe drying trend since 1950 (Held et al. 2005; Hoerling et al. 2006). Observations have shown that a significant drying trend was initiated in the late 1960s and continued through the 1990s (e.g., Dai et al. 2004; Nicholson 2013). Although there has been some recovery of precipitation since 1980s, the rainfall has not returned to the pre-drought level before 1960s (IPCC 2013). The drying (or recovery) is closely related to the drastic reduction (or increase) of the monsoonal rainfall in boreal summer (Giannini et al. 2008). The monsoonal rainy period, also known as the West African Monsoon (WAM), is associated with a seasonal reversal of prevailing winds in the lower atmosphere (southwesterly blowing from June to

✉ Yu-heng Tseng
ytseng@ucar.edu

[1] National Center for Atmospheric Research, P.O. Box 3000, Boulder, CO 80307-3000, USA

[2] Department of Atmospheric Sciences, National Taiwan University, Taipei, Taiwan

[3] Department of Atmospheric Sciences, National Central University, Jhong-Li, Taiwan

September), where humid air is blown in from the Atlantic Ocean and released over the Continent (Nicholson 2013). However, the causes and the factors controlling the spatial distribution of Sahel precipitation and its intensity remain unclear, including the cause of the recent partial recovery (Janicot et al. 2015). Particularly, the associated WAM in boreal summer is characterized as a complicated ocean–atmosphere–land coupling, which is not well understood yet.

Early studies focused on the influence of the overuse of natural resources by humans (e.g. Charney 1975), but later observational and modeling studies have related the Sahel drought with global sea surface temperatures (SSTs) (Folland et al. 1986; Held et al. 2005; Hoerling et al. 2006; Zhang and Delworth 2006; Wang et al. 2012) and land surface processes (Xue et al. 1990, 2010a). The Atlantic Ocean has been long recognized as a major controlling factor of the WAM activity (e.g., Zhang and Delworth 2006). The drying over the Sahel during the boreal summer is affected by the anomalous interhemispheric Atlantic SST contrast, which is characterized by a more southerly position of the Atlantic intertropical convergence zone (ITCZ). Knippers (2003) and Matthews (2004) have suggested that the long-term intraseasonal variability of the WAM may be remotely connected to phenomena as far away as the West Pacific warm pool through the Madden–Julian oscillation. Zhang and Delworth (2006) further suggested that the Atlantic multidecadal oscillation (AMO) plays a primary role in determining rainfall over the Sahel. An AMO warm phase strengthens the boreal summer rainfall over the Sahel, whereas a cold phase diminishes it.

The important role of SSTs on the variability and predictability of west Africa rainfall has been reviewed in Nicholson (2013) and Rodríguez-Fonseca et al. (2015). Recently, Wang et al. (2012) proposed that positive feedback occurs among the North Atlantic tropical SST, Sahel rainfall, and North Atlantic dust. They observed that the drying of the Sahel, which is linked to a cool North Atlantic SST, is associated with periods of increased dust. The transport of dust over the Atlantic serves as positive feedback, which then further cools SSTs (Wang et al. 2012). In general, the observed twentieth-century record results from this drying trend and exhibits substantial internal variability. Aerosols may affect the interhemispheric gradient of SSTs, thereby changing ITCZ locations and precipitation (Chang et al. 2011). In addition, global climate model experiments have shown that tropical convection may shift (e.g., Xue and Shukla 1993) in response to altered vegetation and soil moisture conditions or enhance when subsurface hydrological processes (i.e., groundwater dynamics) exist in the models (e.g., Lo and Famiglietti 2011). These previous works indicated a variety of potential contributions affecting the Sahel rainfall (Nicholson 2013; Rodríguez-Fonseca et al. 2015 and reference therein).

However, experiments in the third phase of Coupled Model Intercomparison Project (CMIP3) and the fifth phase of Coupled Model Intercomparison Project (CMIP5) using multimodel ensembles (MMEs) of forced greenhouse gases have failed to simulate the patterns or amplitudes of twentieth- and twenty-first-century African drying and rainfall variability (e.g., Roehrig et al. 2013). These models even yield inconsistent results regarding the signs of future anomalies in the Sahel (IPCC 2007, 2013). The ensemble spread in the trend amplitude remains large in the Sahel (Roehrig et al. 2013). Several modeling studies have suggested that positive feedback resulting from land–surface interactions and the atmosphere can amplify the climate response to forcings such as SSTs or solar variations (Doherty et al. 2000). Furthermore, the projected rainfall may depend heavily on model resolution and parameterizations, especially in regard to land–atmosphere interactions and representations of convection (Cook 2008; Xue et al. 2010b). Current projections of climate change in the Sahel are inconclusive (e.g., Cook and Vizy 2006; Douville et al. 2006; IPCC 2013). The reasons for contradictions among models have not been determined (Xue et al. 2010b; Roehrig et al. 2013). A major possible cause is built-in model uncertainties associated with MMEs, such as higher degrees of warming and parametric uncertainty (James et al. 2014). The substantial disagreement between these model projections has indicated that certain fundamental mechanisms may be missing in the modeled dynamics (James et al. 2014). The model intercomparison in Roehrig et al. (2013) further indicated the need to separate the issues related to model errors characterized by different time scales, e.g., slow (interannual and longer) and fast (interseasonal or shorter time scale) physical processes. Many systematic errors appear rapidly at the intraseasonal scale.

In order to better clarify the impacts of the uncertainties of the model dynamics, the ensemble simulations based on different initial perturbations within a single model can facilitate exploring the spread of model behaviors and dynamics and have been used commonly in weather forecasts (Zhang 2005; Qian et al. 2013; Feng et al. 2014, 2015). A spread of model behaviors can statistically account for the uncertainties of a complex system. In this study, we performed 1-year short-range ensemble hindcasts initialized from the 6-hourly analysis ensemble prepared by an advanced data assimilation system, the local ensemble transform Kalman filter. With these slightly different initial atmospheric perturbations at each analysis time, we intend to isolate the precipitation biases in the Sahel related to the fast physical processes associated with the fast growing errors, independent of the low frequency impacts of North

Atlantic SSTs. This is the first attempt to determine possible error sources in the Sahel precipitation based on a statistically large amount of data-assimilated ensembles using the NCAR community atmospheric model/community land model while avoiding the additional model uncertainties introduced in MMEs (which are not so easy to quantify due to the large differences in the model physic/grid resolution/parameters). The large number of single model ensembles lends us support to the uncertainties resulting from the dynamical instabilities.

The main objectives of this study are to (a) show that data-assimilated short-range ensemble hindcasts can be used to determine and quantify crucial uncertainties in climate models resulting from the fast physical processes; and (b) confirm that one key dynamic in modeling the Sahel precipitation may be the shifting of the low-level Sahara Heat Low (SHL) associated with the African easterly jet (AEJ) suggested in many previous studies (e.g., Biasutti et al. 2009; Xue et al. 2010b; Diallo et al. 2013, 2014; Cook 2015). This approach can isolate an important source of model errors/uncertainties resulting from the dynamic processes triggered in the low-level boundary layer (BL) rather than other model uncertainties. To the best of our knowledge, this study is the first to clearly demonstrate and identify that the internal variability due to the fast process dynamics (within several months) can significantly contribute to the uncertainty of a climate model in the Sahel precipitation. From these ensemble simulations, we confirmed the modeled location and amplitude of the SHL and AEJ are critical while their associated dynamics are influenced by the temperature gradient in the low-level BL and enhanced by land–atmosphere interactions. This source of biases has been suspected in the previous MMEs (Biasutti et al. 2009) but cannot easily be identified.

The rest of the paper is organized as follows. Section 2 describes the methods used in the current study. Section 3 discusses the results of the ensemble simulations in 2000. Section 4 investigates the relevant land–atmosphere interaction, followed by the atmospheric circulation in Sect. 5. Finally, the discussion and conclusion are given in Sect. 6 and 7.

2 Methods

2.1 Short-range data-assimilated ensemble hindcasts

We conducted the short-range ensemble hindcasts by using the NCAR Community Atmosphere Model (CAM3.5) with the Community Land Model (CLM3.5), a prognostic atmospheric model with detailed land–surface feedback within the Community Climate System Model framework (Gent et al. 2010). CAM3.5 is based on a global primitive

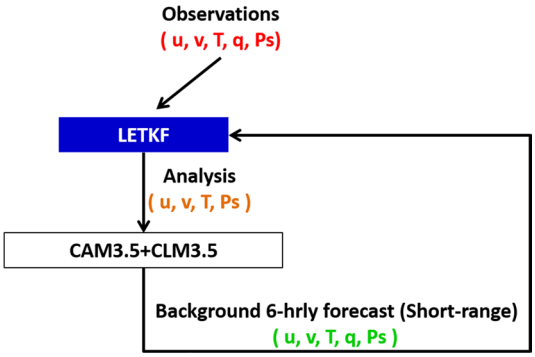

Fig. 1 Overview of the data-assimilated CAM3.5/CLM3.5 hindcast system

equation model with 26 vertical levels. The model integration uses a finite-volume dynamical core and the horizontal resolution is approximately 2.5° longitude by 1.9° latitude (144 × 96 longitude-latitude grid). CAM3.5 (the precursor of the recently released CAM4 and CAM5) exhibits improvements in modeling of tropical convection, surface winds, Hadley circulation, tropical easterly winds, subtropical westerly winds, and related precipitation fields through new convective momentum transports (see Neale et al. 2008; Richter and Rasch 2008 for further details). CLM3.5 has an improved hydrological cycle, particularly in its partitioning of global evapotranspiration and an improved annual cycle of total water storage and runoff (Oleson et al. 2008; Stockli et al. 2008).

A local ensemble transform Kalman filter (LETKF, Hunt et al. 2007) has been coupled with the CAM3.5/CLM3.5 model and assimilates meteorological data every 6 h (Liu et al. 2009, 2012), hereafter CAM-LETKF. The dataset includes all operationally assimilated observations used in DOE/NCEP Reanalysis II (Kanamitsu et al. 2002), including vertical sounding temperature and wind profiles obtained from weather balloons, surface pressure observations obtained from land and sea stations, temperature and wind reports obtained from commercial aircraft, and wind vectors obtained from the satellite-based observation of clouds. An ensemble hindcast system with 64 members has been established using the CAM-LETKF analysis ensemble as the atmospheric initial conditions. Figure 1 shows the flowchart of the CAM-LETKF assimilation system. We note that except the moisture variable, all prognostic variables were updated at each analysis time. The moisture is not updated because it directly linked with the precipitation. This ensures the precipitation mechanism in the ensemble hincasts can be initialized through the model dynamics rather than the direct assimilation. The detailed data-assimilated hindcast system has been discussed in Liu et al. (2009, 2012).

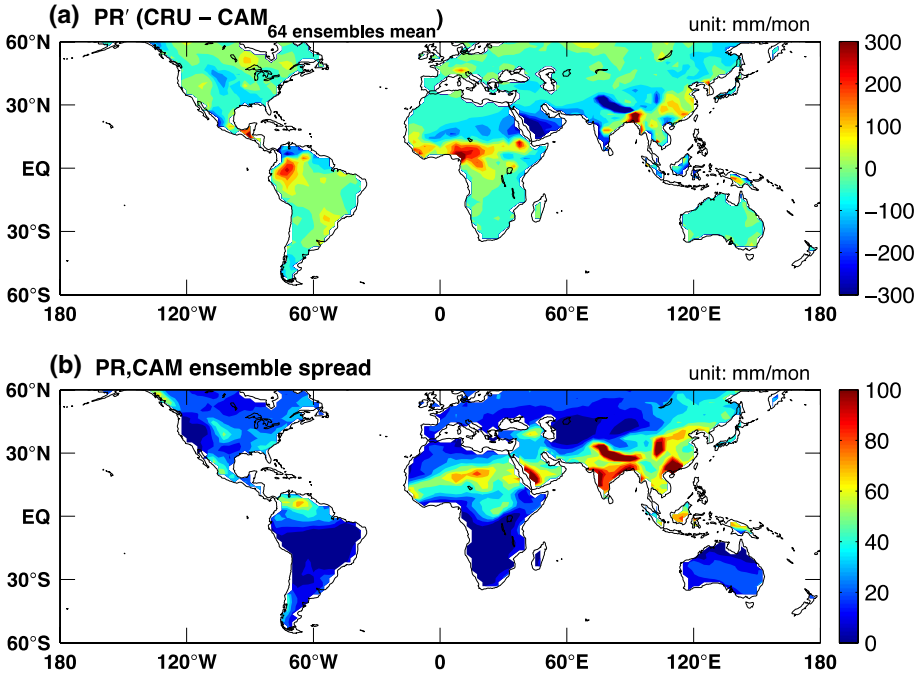

Fig. 2 **a** Precipitation biases of the 64 ensemble mean comparing with the CRU data in August, 2000. **b** Standard deviation (ensemble spread) of the 64 ensembles from (**a**)

A 6-hourly short-range ensemble simulation, initialized from the CAM-LETKF analysis ensemble every 6-h, is used to evaluate African precipitation in the boreal summer. We conduct the 6-hourly ensemble hindcasts for 1 year from January 2000 to December 2000 in order to identify the short-term fast process affecting the dynamics of African climate, independent from the well-known slow process resulting from the impacts of low-frequency North Atlantic SSTs. Year 2000 is chosen arbitrarily while the ensemble hindcasts can be used for any year. Although multi-year experiment can yield a more robust result, 1 year is sufficient to emphasize the particular dynamics discussed here. The short-range ensemble hindcasts are used to avoid issues related to unbalance, model spin-up, slow process dynamic and potential long-term climate drift. Also, distinguished from the other studies using long-range simulation initializing, these ensemble hindcasts contain natural variability brought in by frequent data assimilation and thus we referred it to short-range ensemble hindcasts. The current approach is unique and statistically crucial in determining the ensemble differences triggered by the 6-hourly perturbations in the atmospheric field exclusively. Overall, we take the advantage of an existing CAM-LETKF system to generate the ensemble hindcasts and its quality has been evaluated in Liu et al. (2011, 2012). Figure 2a shows the ensemble mean biases of precipitation comparing with the CRU data in August 2000. The model's accumulated precipitation is used here. The largest model biases occur in the north part of South America and the Sahel, which extends to the Arabian Peninsula and south Asia. The distribution of the global precipitation biases is quite consistent with the large ensemble spread among these ensembles (Fig. 2b).

We note that the difference among ensembles is important since it represents the dynamical uncertainties which can quickly grow within several months. Aiming at perturbing the dynamic/thermodynamic components of the initial conditions, some methods like breeding vectors (Toth and Kalnay 1993, 1997), singular vectors (Buizza et al. 1997) and ensemble transform perturbations (Wei et al. 2008), are commonly used for weather or climate ensemble prediction. These approaches can effectively detect the uncertainties related to dynamical/thermodynamic instability mechanism. Due to the various characteristics of the perturbations from different ensemble initialization schemes, these initial perturbations can lead to different error growth and different performance of the ensemble prediction system. In terms of representing the short-term forecast errors, Bowler (2006) suggests that the ensemble Kalman filter is the best framework for generating initial condition perturbations. Studies with global ensemble prediction system show that different ensemble initialization schemes lead/converge to similar performance in the well-observed areas (e.g. North hemisphere), while methods using nonlinear models like the bred vector and EnKF perturbations exhibit better prediction skill in tropics (Magnusson et al. 2008; Buehner and Mahidjiba 2010).

The LETKF background ensemble is derived by using a nonlinear model and thus the growth of the ensemble perturbations is dominated by nonlinear dynamical/thermodynamic instabilities. Also, assimilating observations reduces the discrepancies among ensemble members. Similar to the breeding

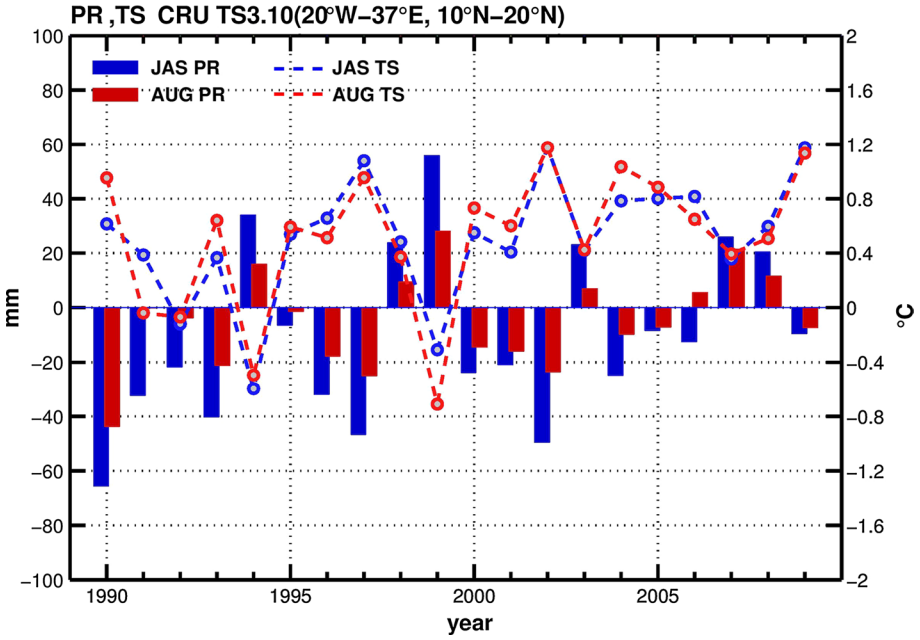

Fig. 3 Time series of the observed CRU TS3.1 total rainfall (*bars*) and mean temperature (*lines*) departures based on the mean of 1950–1990 for JAS (July, August, and September) and August only over Sahel since 1990 (20°W–37°E, 10°N–20°N). Correlation is −0.70 and −0.84 for the period of 1990–2009 and 1950–2009, respectively

method, the LETKF is also regarded as a nonlinear approach to generate dynamically-related perturbations, except that the rescaling is done by assimilating observations compared to a constant rescaling factor used in the breeding method (Kalnay and Toth 1994; Corazza et al. 2003; Yang et al. 2006; Hoffman et al. 2009). The current approach is completely different from the MMEs, which intend to represent the model uncertainties. We emphasize that the differences in dynamics, physics, initial conditions, boundary conditions, and resolution, and other minor differences among MMEs may further increase model uncertainty, which is difficult to quantify (James et al. 2014). This approach also differs from that used in the CESM large ensemble climate project (https://wiki.ucar.edu/display/ccsm/CESM+Large+Ensemble+Planning+Page), in which large members of long-term free model simulations that vary in initial perturbations resulting from random error are used. The large-ensemble climate project encompasses a substantial group of free model simulations without any constraints; by contrast, our 64 ensemble members are strongly constrained by observations over time through the short-range ensemble hindcasts initialized by frequently updated analysis ensemble. Thus, the modeled dynamics may not largely diverge from the observed dynamics. Direct comparisons with observations can be more effectively justified and any particular process which may lead to the poor performance of prediction can be easier diagnosed by using our ensembles than the CESM large ensembles and MMEs.

2.2 Observational data

The Climate Research Unit (CRU) TS3.1 dataset is used in this study in addition to the short-range ensemble hindcasts. The CRU TS3.1 is the global dataset of the monthly gridded 0.5° × 0.5° precipitation and temperature for the period 1901–2009. The gridded dataset is based on archival data from more than 4000 weather stations distributed around the world. Each station observation was constructed based on anomalies from the mean of the period 1961–1990 for that station. The precipitation and mean temperature used here were interpolated directly from station observations as a function of latitude, longitude, and elevation. All results shown here remain unchanged when the Global Precipitation Climatology Project (Adler et al. 2003), CPC Merged Analysis of Precipitation (Xie and Arkin 1996) and other version of CRU datasets were used as precipitation observations. This indicates the global model biases in the Africa are much larger than the disagreement among different observations and datasets.

3 Results of the short-range ensemble hindcasts in 2000

Figure 3 shows 1950–2009 time series of observed CRU TS3.1 rainfall (bars) and temperature (lines) departures based on the mean for July–September 1950–1990 (JAS, blue) and August only (red) over Sahel (20°W–37°E, 10°N–20°N). The observed precipitation in the Sahel was highly correlated with the temperature variation (corr. is −0.70 and −0.84 for the period of 1990–2009 and 1950–2009, respectively), indicating that the variability of Sahel precipitation is closely associated with Sahel temperature variability in recent decades. Although the Sahel precipitation has gradually recovered from its very dry periods since

Table 1 List of individual members in the first (and the last) two groups with the minimum (and maximum) error in precipitation and temperature

No.	Group 1				Group 2			
Precipitation	***34***	***19***	61	***4***	60	42	**48**	**43**
Temperature	***19***	***4***	***34***	**43**	32	62	21	**48**
No.	Group 15				Group 16			
Precipitation	40	**20**	**15**	17	**50**	***6***	33	**31**
Temperature	**31**	59	**50**	53	45	**15**	**20**	***6***

Group 1 is the group of the minimum error and group 16 is the group of the maximum error. The *italic* numbers appearing in Groups 1 (and 16) are the overlapping members for both precipitation and temperature. The bold numbers mark members that appeared in both precipitation and temperature when Groups 1 and 2 (and 15 and 16) were considered

late 1980s, lower-than-average precipitation and higher temperatures in Sahel still occurred in 14 out of 20 years after 1990.

The forward CAM3.5/CLM3.5 results are used here instead of the analysis fields. We sorted the 64 members into 16 groups based on the root-mean-square errors of precipitation/temperature in African continent compared with the CRU TS3.1 dataset (the errors between model results and the interpolated observation) in August 2000. All model comparisons made in this study are based on the average of the whole African continent for consistency although the major biases occur in Sahel (discussed later). Considering the whole African continent allows us to evaluate the distribution of biases and the associated atmospheric circulation difference which is not confined to the Sahel only. Group 1 exhibited the minimum error, whereas Group 16 exhibited the maximum error. The results were extremely robust regardless of the observational datasets used for comparison. Eighty percent of the annual rainfall in the Sahel occurs during the 3-month period of July–September (Lebel et al. 2003). August is the wettest month and it contributes disproportionately to the interannual variability (Nicholson and Palao 1993). Hereafter, we only focus on August 2000 since the WAM often onsets in June and reaches its matured phase in August, resulting in the most robust model–data comparison in the precipitation and temperature that month.

The individual members within Groups 1 and 2 and Groups 15 and 16 are tabulated in Table 1 for precipitation and temperature, respectively (ranked based on the minimal to maximum errors). Many members in the group of the minimum (and maximum) error are the same. For example, member 4, 19 and 34 in the minimal error group 1 can be found for both precipitation and temperature fields (*italic* members in the Table 1); same as member 6 in group 16 (maximal error). Approximately one half of the members of Groups 1 and 2 (and the members of Groups 15 and 16) that exhibited the minimum (and maximum) error in either precipitation or temperature were the same members (Table 1; bold members), indicating that more accurate simulations typically generate more accurate precipitation and temperature fields and that both fields are closely connected. Better simulation in the precipitation field is often associated with better temperature simulation and vice versa. The settings of these ensembles were identical, except the 6-hourly atmospheric perturbations (wind vectors, temperature, and surface pressure) during each data-assimilation cycle. The classifications in Table 1 led us to select five superior and five inferior members that exhibited the best precipitation and temperature (minimum errors in both fields) from Groups 1 and 2 and the poorest precipitation and temperature fields (maximum errors in both fields) from Groups 15 and 16, respectively. Figure 4a, b show the mean observed precipitation and temperature, respectively, based on CRU TS3.1 in August 2000. Figure 4c, d show the superior group of CAM3.5/CLM3.5 during the same period, and Fig. 4e, f show the inferior group. The modeled rainbelt location and temperature distributions in the superior group were highly consistent with observations, except the strength of the modeled rainbelt was weaker and the modeled mean temperature was slightly cooler than those observed in the Sudanian Savanna. The modeled rainbelt in the inferior group shifted northward in comparison with observations. All hindcasts appeared to have a systematically warm temperature bias in Egypt near the south coast of the Mediterranean Sea, although this warm bias decreased slightly in the superior group.

Figure 5a, c show the differences between the superior and inferior groups in mean precipitation and temperature, respectively, in August 2000. The ensemble means for precipitation and temperature are shown in Fig. 5b, d, respectively. The two groups were significantly different by more than 60 mm in precipitation and 1.5 °C in temperature in a large area (particularly North Africa), confirming the large ensemble spread in the Sahel seen in Fig. 2b. The precipitation difference was comparable to the overall August mean precipitation variability in the Sahel (Fig. 3). These results suggested a large model uncertainty in this region and implied a significant difference in atmospheric responses and dynamics among these members even though the

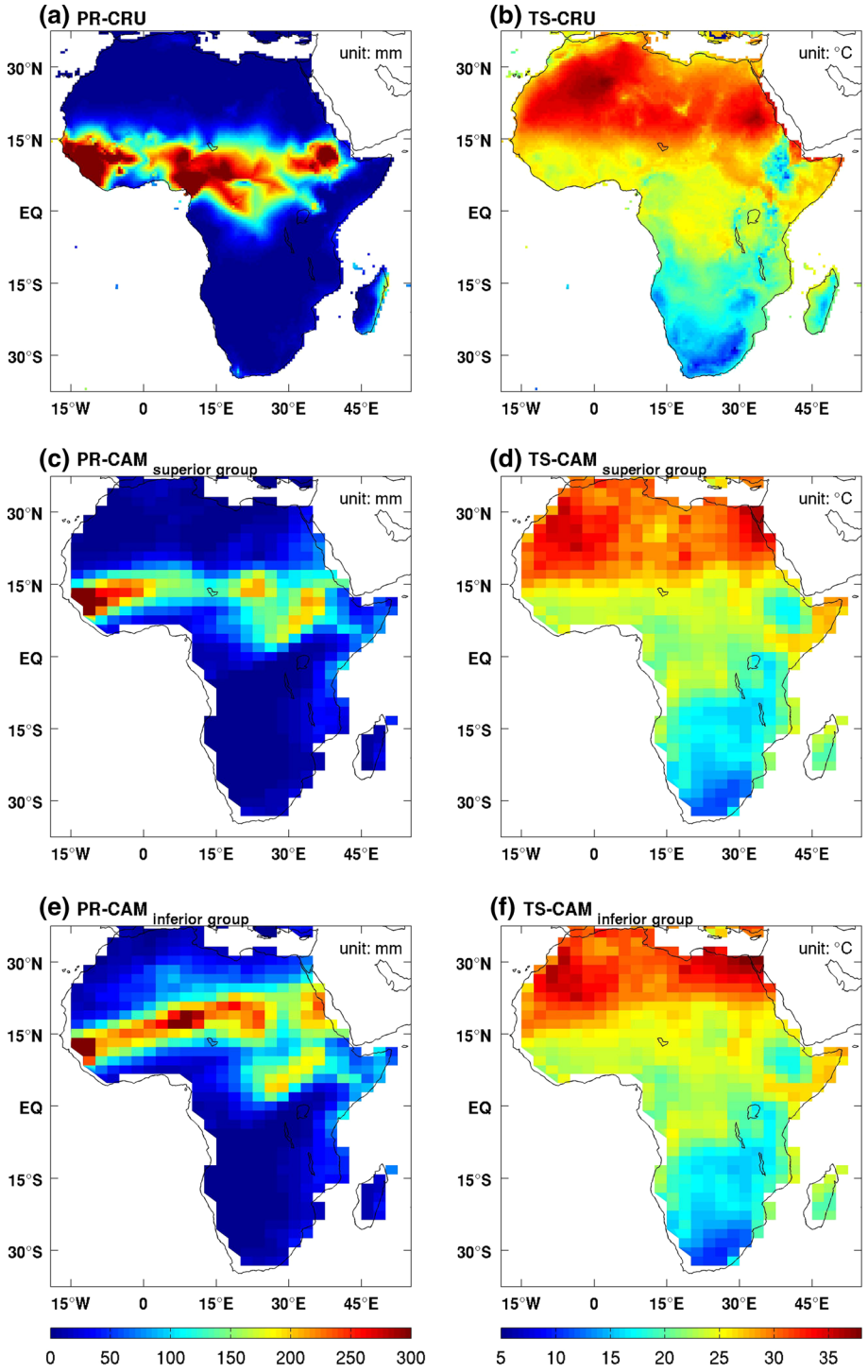

Fig. 4 Mean precipitation and temperature based on the observed CRU TS3.1 dataset **a** precipitation and **b** temperature; **c**, **d** are the same as **a**, **b** but from the superior group of CAM3.5/CLM3.5; **e**, **f** are the same as **a**, **b** but from the inferior group of CAM3.5/CLM3.5

ensemble hindcasts are forced using the same surface boundary conditions and settings. The detailed error distribution of these ensembles is presented in rank histograms of precipitation and temperature in Fig. 6a, b, respectively.

Based on these ensembles, we further analyzed the probability of error estimation for the Sahel precipitation. A significant mean bias of 88 mm in precipitation and 3 °C in temperature for Africa was observed in comparison with the CRU TS3.1 dataset (solid lines in Fig. 6). In addition, the model spread (the standard deviation was 10.15 mm and 0.16 °C for precipitation and temperature, respectively) was much smaller than the mean bias (dashed lines in Fig. 6), indicating that the short-range ensemble hindcasts retained various systematic model biases. Some inherent model biases cannot easily be corrected. However, the range of the model spread was large (approximately 50 mm

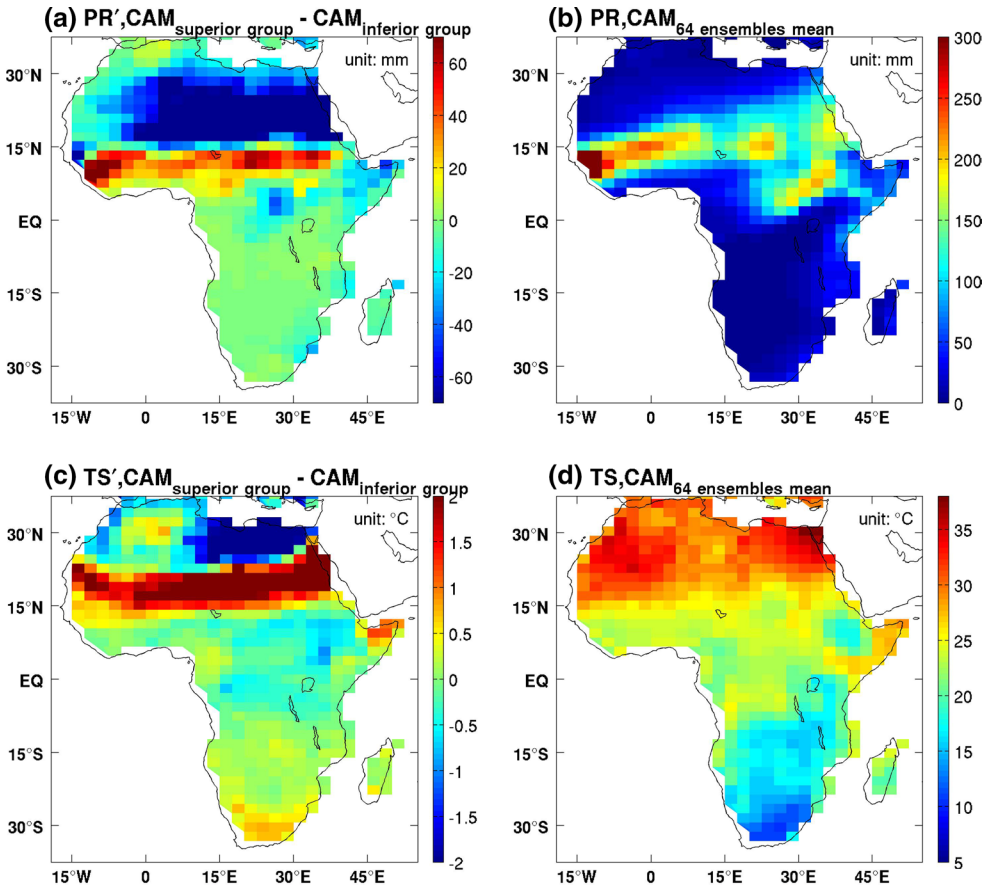

Fig. 5 **a** Mean precipitation and **c** mean temperature differences between the superior and inferior groups in August 2000, and the mean of 64 ensemble members in **b** precipitation and **d** temperature in August 2000

in precipitation and 1 °C in temperature). These differences in the model spread revealed that the modeled mean rainbelt might generally shift toward the Sahara desert, possibly because of the northward shift of the modeled ITCZ in Africa. This particular bias can lead to an erroneous interpretation if the uncertainty is not carefully quantified and identified in the long-term integration.

By comparing the error introduced by any ensemble member with the ensemble mean error, we may quantitatively define the error reduction/increase for each member, i.e., $(\varepsilon_m - \varepsilon_{EM})/\varepsilon_{EM}$, where ε_m is the error for any individual member m and ε_{EM} is the ensemble mean error. The optimal simulation in Group 1 can reduce the mean systematic error in precipitation by up to 25 % and that in temperature by 16 %. These results were consistent with the error ranking in Table 1 and motivated us to further investigate how these better rainbelts could be achieved in the superior hindcasts.

4 Land–atmosphere interaction

Our analysis showed that modeled precipitation and temperature in the Sahel can differ substantially in structure with the same model setup and configuration. We first investigated whether this large difference resulted from land–atmosphere interactions. The Sahel region is located in a transition zone between wet and dry climates where the atmosphere and land surface are strongly coupled (e.g., Entekhabi and Rodriguez-Iturbe 1994; Eltahir 1998; Koster et al. 2004; Xue et al. 2010a). In other words, land–atmosphere interactions may exert a substantial impact on precipitation anomalies. However, a comprehensive understanding of the land–atmosphere interactions and feedback system in the Sahel has yet to be attained. The short-range ensemble hindcasts indicated that soil moisture exhibited positive responses to rainfall and was likely linked to the difference between the superior and inferior groups.

Figure 7a shows that the pattern of soil moisture differences between the superior and inferior groups resembles to the pattern of precipitation differences as shown in Fig. 5a. Less (more) soil moisture in the superior group was associated with less precipitation north (south) of 15°N. The general pattern of soil moisture differences between the superior and inferior groups was also similar to the pattern of the latent heat flux differences (Fig. 7b) due to the decreased (increased) evaporation north (south) of 15°N in the superior group. In the superior group, the reduction in the total turbulent heat flux north of 15°N caused by decreases in soil moisture tended to reduce the net surface radiation because of warmer surface temperature. The warmer surface

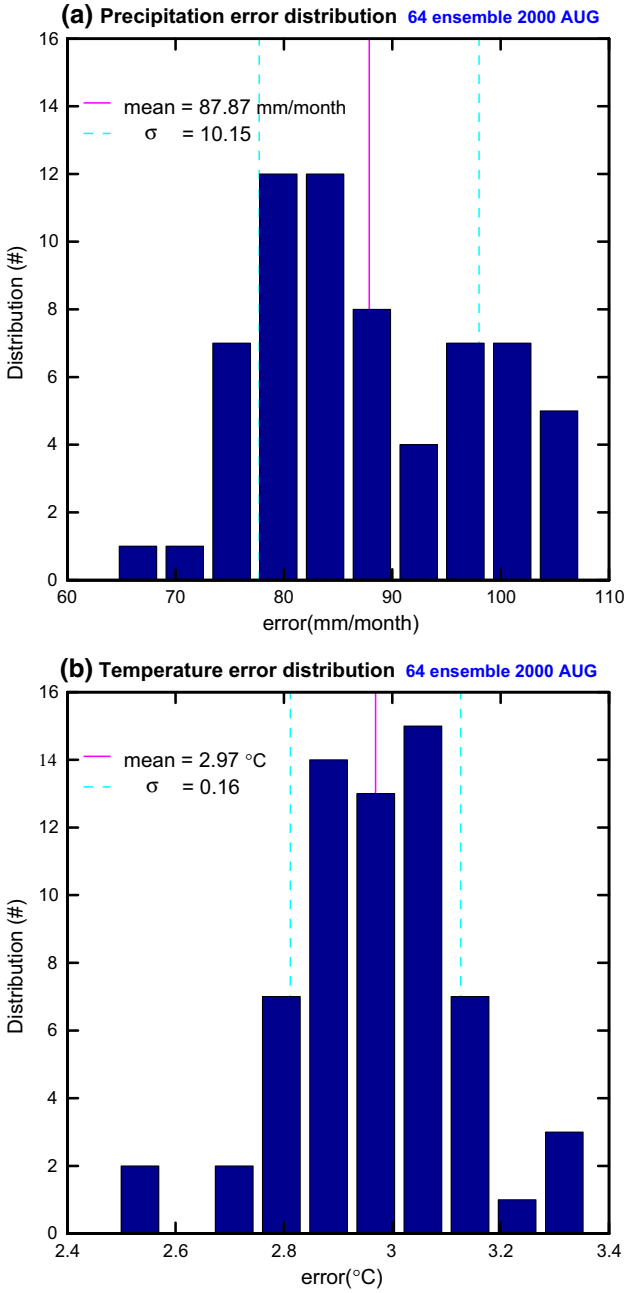

Fig. 6 Error distribution of the 64 ensemble simulations for **a** precipitation and **b** temperature. The *solid line* represents the ensemble mean and the *dashed line* represents the range of one standard deviation

temperature and enhanced upward longwave radiation simultaneously reduced the atmospheric water vapor content (not shown here). Thus, precipitation north of 15°N was significantly reduced in the superior group.

In addition, we can find the change in latent heat flux (evaporation) dominated the total turbulent heat flux (Fig. 7d) at the surface in the ensembles as expected. The pattern of sensible heat flux anomalies (Fig. 7c) was not similar to that of the latent heat flux (Fig. 7b), possibly because of the impacts of cloud and net radiation. The Bowen ratio was substantially different in central to eastern Africa within 15°N–30°N between the superior and inferior groups (Fig. 8). The largest precipitation difference was observed in this region. In the superior group, the sensible heat flux was significantly larger than the latent heat flux (higher Bowen ratio), but in the inferior group, the Bowen ratio was small. In all other regions, the general patterns of the Bowen ratio were quite similar. The results shown in Figs. 7 and 8 clearly indicated the immediate response of land processes (positive feedback) to the simulated precipitation in the superior and inferior groups.

Although the positive land–atmosphere feedback amplifies the precipitation differences locally as shown in Fig. 7, we did not expect the difference in precipitation patterns between the superior and inferior groups to match the difference in temperature between the two groups exactly because other systematic biases may have existed and could not be easily identified here. For example, the major bias in the mean modeled temperature pattern was located near the south coast of the Mediterranean Sea, where warm biases are commonly observed in the ensembles (comparing Figs. 4b, 5d). Although the superior group exhibited a slightly better temperature field than the inferior group in this region (perhaps because of the improved rainbelt in the south), the improved result seemed not to be fully related to the dominant cause of the precipitation and temperature biases.

These results suggested that the thermodynamic land–atmosphere coupling in both Sahel and north of the Sahel (north of 15°N) is related to the significant differences in precipitation and temperature between the superior and inferior groups. We note that the only difference in these ensemble hindcasts was the initial atmospheric conditions. Every 6-h, the CAM-LETKF system updated the ensemble-hindcasts with flow-dependent analysis corrections. These corrections are related to the atmospheric instability in the underlying flow and the distribution of observation. Thus, the ensemble differences can be constrained and appear in the dynamically sensitive areas. The atmospheric model passively drove the land model through two-way coupling. This implied that the role of land–atmosphere interactions in this region, in the current ensemble hindcasts, exerted more of an amplification rather than a triggering effect. The triggering of land–atmosphere amplifications likely occurred in low-level atmospheric fields.

5 Atmospheric circulation

Because the superior group exhibited considerably fewer systematic errors (improving 25 % in precipitation and 16 % in temperature), we further evaluated whether any

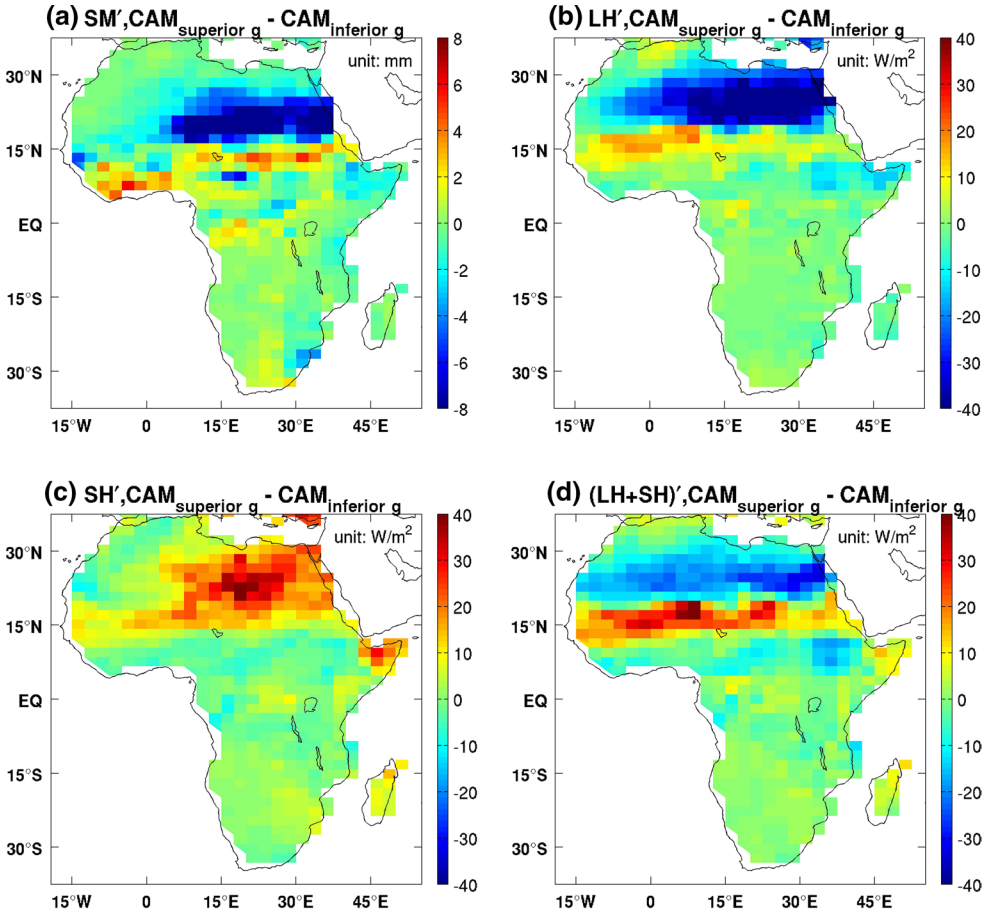

Fig. 7 Differences between the superior and inferior groups in **a** soil moisture, **b** latent heat flux, **c** sensible heat flux, and **d** latent and sensible heat flux in August 2000

significant changes in the atmospheric circulation among the ensembles occurred; in particular, the differences between the superior and inferior groups. The left panel of Fig. 9 shows the divergence superimposed by the associated wind field at (a) 850 mb, (c) 600 mb, and (e) 200 mb for the superior group in August 2000. The differences between the superior and inferior groups are shown in the right panel: (b) 850 mb, (d) 600 mb, and (f) 200 mb. These differences are of the same order as the mean fields, indicating that significant changes indeed occurred in the mean atmospheric fields.

Based on the wind field at 850 mb, we see the low-level westerlies (or called southwesterly monsoon flow) originate in the Gulf of Guinea and transport northwestward (Fig. 9a), feeding on moisture advected from the tropical Atlantic. This is confirmed in Fig. 10a, b, showing the SST (color) and sea level pressure (SLP) in August 2000 in the superior and inferior groups, respectively. Since the model is forced by the oceanic SST, the dataset of National Oceanic and Atmospheric Administration optimum interpolation SST analysis (Hurrell et al. 2008) used in the CAM-LETKF system is presented here. The modeled SLP is superimposed by contours in Fig. 10a, b. The difference of SLP between these two groups is also shown (color) in Fig. 10c, superimposed by the 850 mb wind vector difference. Note that the difference of SLP is very similar to the difference of surface pressure (not shown here). The use of SLP rather than surface pressure is mainly due to its smoother transition in the ocean–land interface. We can clearly see no significant difference above the ocean while a noticeable difference can be found just north of the Sahel, leading to the differences in the 850 mb wind vectors. The humid air south of the ITCZ arises as the southeasterly trades cross the Equator and takes on a westerly course (Nicholson and Webster 2007), as shown in Fig. 9a. The moisture is driven by the boreal summer ocean–continent temperature contrast, which causes a substantial change in direction regarding the large-scale flow, driving ocean moisture far inland and causing the summer African rainfall.

The westerly monsoon flow of WAM can be seen mostly in the low levels of the troposphere in Fig. 9a (not seen at 600 and 200 mb). This westerly jet (the African westerly jet, AWJ) is strong at 850 mb and typically extends into the midtroposphere in boreal summer (Nicholson and Webster 2007). Figure 9b shows the AWJ in the superior group is much weaker than that in the inferior group, making the largest difference at 850 mb. This AWJ variation has been

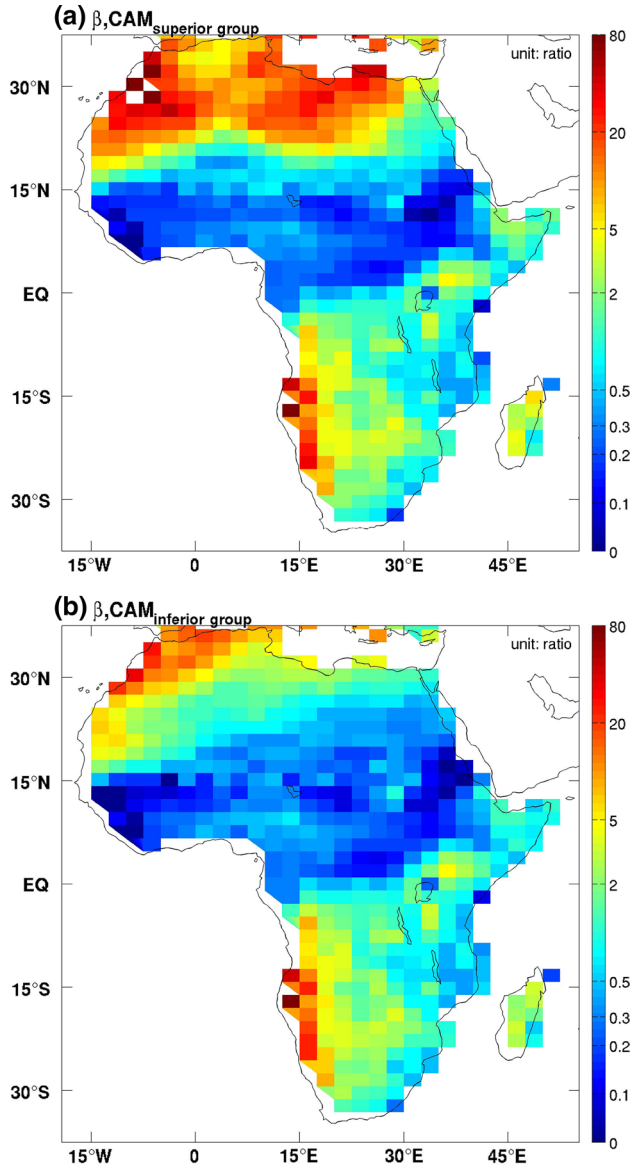

Fig. 8 Spatial patterns of the Bowen ratio for the **a** superior group and **b** inferior group. A log scale is used to emphasize the broad range of the Bowen ratio

strongly linked to the interannual variability of West African rainfall. The differences in the ocean and South Africa are almost inappreciable, confirming that the model consistently simulates the impact of the Atlantic Ocean on the WAM to drive the AWJ regardless superior and inferior groups (but the strengths vary). This is further supported by the difference of the meridional surface temperature (contours) and SLP (color) gradients between the superior and inferior groups (Fig. 10d). The meridional surface temperature (or SLP) gradient is calculated by the meridional surface temperature (or SLP) difference divided by the grid distance in meter. The contour intervals are 2×10^{-6} °C/m (negative is dashed and positive is solid). No substantial differences can be found at the ocean surface, suggesting the consistent ocean driving forcing among these ensembles and the oceanic influence (related mostly to the interannual variability which is not addressed here) does not seem to be the dominant forcing that triggered the ensemble differences. However, significant differences appear more likely in the lower troposphere of Sahel.

In the superior group, the AEJ could be seen at 600 mb but not clear at 850 mb (the observed maximum was near 600–650 mb in the midtroposphere) in Fig. 9a, c. It is closely connected with the development and propagation of wave disturbances (e.g., the African easterly wave) over West Africa (e.g., Burpee 1972). The enhanced AEJ in the superior group comparing with the inferior group was associated with the increase of convergence in the band between 7°N and 15°N (Fig. 9b, d), potentially resulting in an enhanced precipitation found in Figs. 4 and 5. The modeled strength and location of the AEJ seemed to play a crucial role in modulating the divergence field at 850 mb and, thus, linked with the systematic precipitation and temperature biases in CAM3.5/CLM3.5. This was consistent with the upper troposphere divergence in the Sahel (Fig. 9e) and associated with a weakened tropical easterly jet (TEJ) in the superior group.

The comparisons of August precipitation with observation in Figs. 4 and 5 showed that the largest precipitation region (the typical tropical rainbelt) could only be accurately reproduced in a few of the ensembles (i.e., the superior group). The primary rain-producing mechanism in August is the strong core of the ascent between the axes of the AEJ and TEJ, which controls the large-scale tropical rainbelt in the boreal summer (Nicholson 2009). Figure 9 indicated that the modeled ensemble mean (or particularly the inferior group) AEJ and TEJ generally shifted northward because the TEJ is too strong near equator and the AEJ is too weak at north, producing erroneous rainfall in the Sahara rather than in the central and southern Sahel (10°N–15°N). These jets' location dominated the band of divergence and convergence, suggesting that the jet dynamics directly affect precipitation in the Sahel in August.

The observed main rainbelt was located slightly south of the ITCZ, which is characterized by surface convergence (Fig. 9). From the SLP difference between the superior and inferior groups (Fig. 10c), we can see a strong anomalous pressure high, which corresponded to a reduction in the SHL, occurred north of 15°N in the superior group and was associated with anticyclonic wind fields resulting from the enhanced AEJ in the superior group. Thus, in the superior group, this anomalous circulation pattern enhances the precipitation in the Sahel with reduced precipitation in the Sahara, shifting the main rainbelt southward to the correct location. Interestingly, similar southward shifting bias of SHL was also reported in the regional model (Diallo et al.

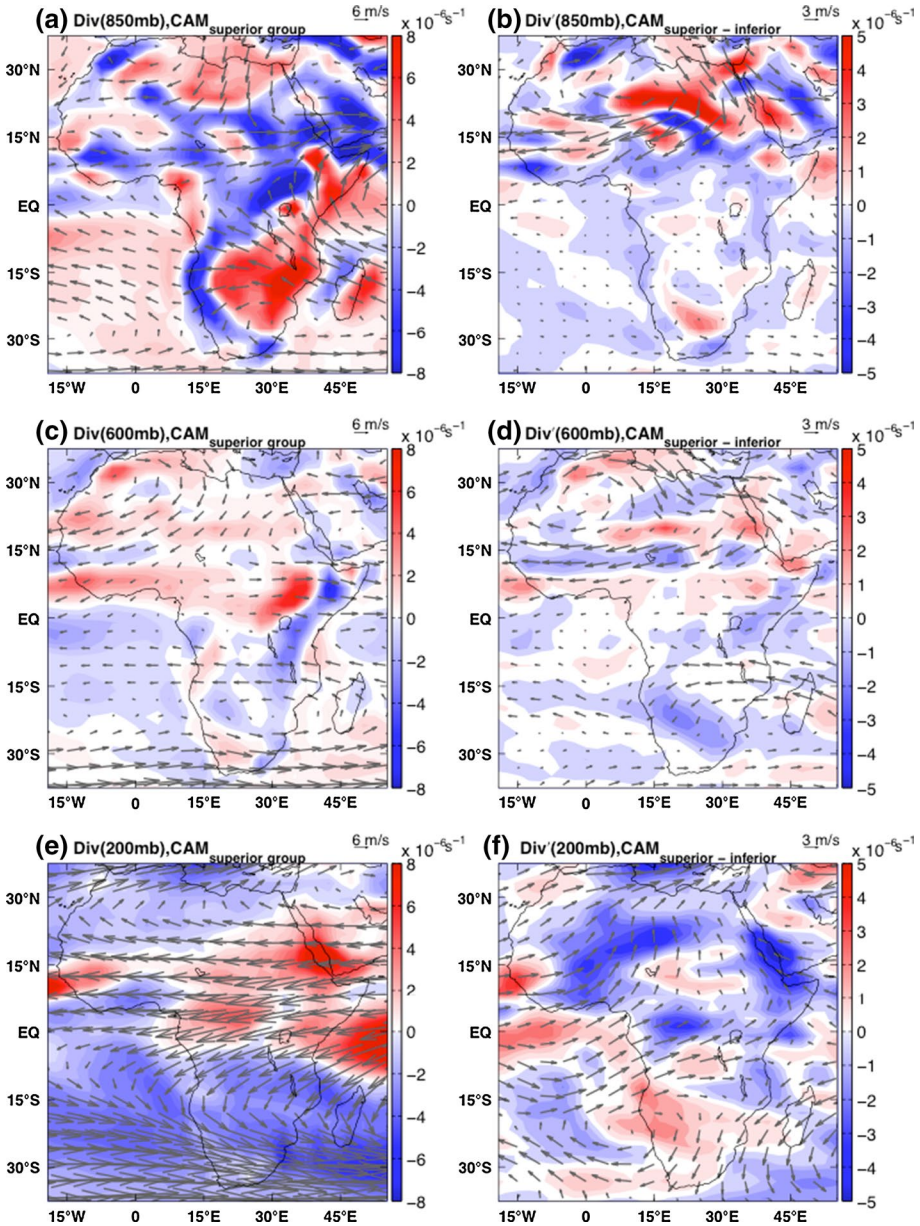

Fig. 9 Divergence superimposed by the associated wind field at **a** 850 mb, **c** 600 mb, and **e** 200 mb for the superior group in August 2000. The differences between the superior and inferior groups are shown at **b** 850 mb, **d** 600 mb, and **f** 100 mb

2014) and global model (Vellinga et al. 2013), indicating a possibly consistent structure uncertainty in the model dynamics.

This analysis prompted a key question: what causes the shifting of the AEJ and changes the SHL in the ensemble hindcasts? Many previous studies have proposed that these changes result from the land surface (e.g., Giannini et al. 2008). Our analysis in Sect. 4 suggested that land–atmosphere interactions may only serve as an amplifier rather than as the actual cause. Moreover, the rainfall and surface temperature variability is extremely sensitive to the modeled vertical structure of the atmosphere, where the divergence field plays a key role in precipitation (Nicholson 2009). Figure 11a shows the distribution of the meridional temperature gradient in August along 12.5°N in the superior group, which indicates a clear temperature gradient maximum in the lower troposphere over Africa (15°W–50°E). The positive temperature gradient extended from the surface to 600 mb. Above 600 mb, the temperature gradient was reversed by a weak negative gradient. Figure 11c shows the differences in the meridional temperature gradient between the superior and inferior groups. The largest difference (and probably the only difference) clearly resulted from the low-level BL over Africa, where land–atmosphere interactions occur (900–700 mb approximately). This further confirms that land–atmosphere feedback may play a crucial role in amplifying unstable modes

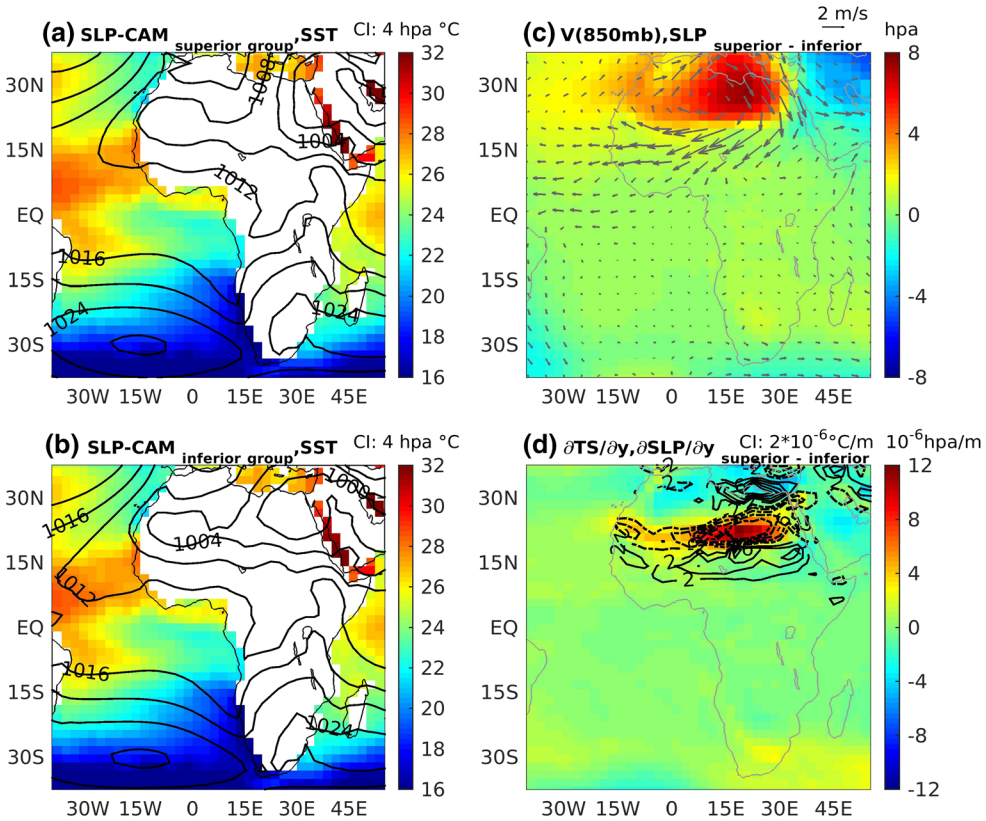

Fig. 10 **a** SST (*color*) and SLP in August 2000 for the superior group. The SLP is superimposed by contours. **b** Same as **a** but for the inferior group. **c** SLP difference (*color*) superimposed by the 850 mb wind vector difference between the superior and inferior groups. **d** The difference of meridional SLP (*color*) gradients between the superior and inferior groups superimposed by the meridional surface temperature gradient (contours with contour interval 2×10^{-6} °C/m, negative is *dashed* and positive is *solid*)

in the low-level BL, resulting in large differences in the temperature gradient and zonal velocity.

Figure 11b, d show vertical sections of the zonal velocity averaged over West Africa (15°W–5°E) for the superior group and the difference between the superior and inferior groups, respectively. The TEJ (centered at 200 mb) and a weak AEJ (centered at 600 mb) were observed in the superior group (Fig. 11b). The AEJ is geostrophic because of the existence of a positive surface temperature gradient, which, according to the thermal wind relation, induces easterly shear over the surface monsoon westerlies. The enhanced AEJ in the superior group (compared with the inferior group, see the difference in Fig. 11d) was initiated by the strong vertical shear generated at approximately 800 mb, which is consistent with the largest temperature gradient. These results indicated that the low-level temperature perturbation was amplified and increased through local land–atmosphere feedback, resulting in the major differences between the superior and inferior groups. The large differences in the atmospheric temperature gradient influenced the location and magnitude of the AEJ and, thus, affected the location and strength of the SHL. Because the changes in the AEJ and SHL can cause significant changes in low-level heating (Cook 1999), the better atmospheric circulation in the superior group may have facilitated more accurate divergence and convergence fields, thus resulting in better rainbelt location through a positive feedback.

6 Discussion

Precipitation in the Sahel has drawn a considerable amount of attention in the recent decades because of the well-known Sahel drought. Several mechanisms have been proposed by researchers such as Neelin et al. (2003), Chou and Neelin (2004), Held et al. (2005), and Giannini et al. (2008). However, neither the SST nor the land–sea thermal contrast alone can straightforwardly explain model variations/uncertainties in the future trends predicted for rainfall in the Sahel. Based on the CMIP3 model results, Biasutti et al. (2009) suggested that the discrepancy in the model projections for twenty-first-century Sahel precipitation are directly related to the variability of SHL anomalies at interannual to centennial time scales. Without using a long-term integration, our diagnosis of ensemble hindcast in 2000 supported that more accurate prediction of the location and amplitude of the SHL associated with the AEJ improved predictions of boreal summer Sahel rainfall by more than 25 % in precipitation and 16 % in temperature (comparing the optimal simulation in the Group 1 and the ensemble mean). This is also consistent with the recent model

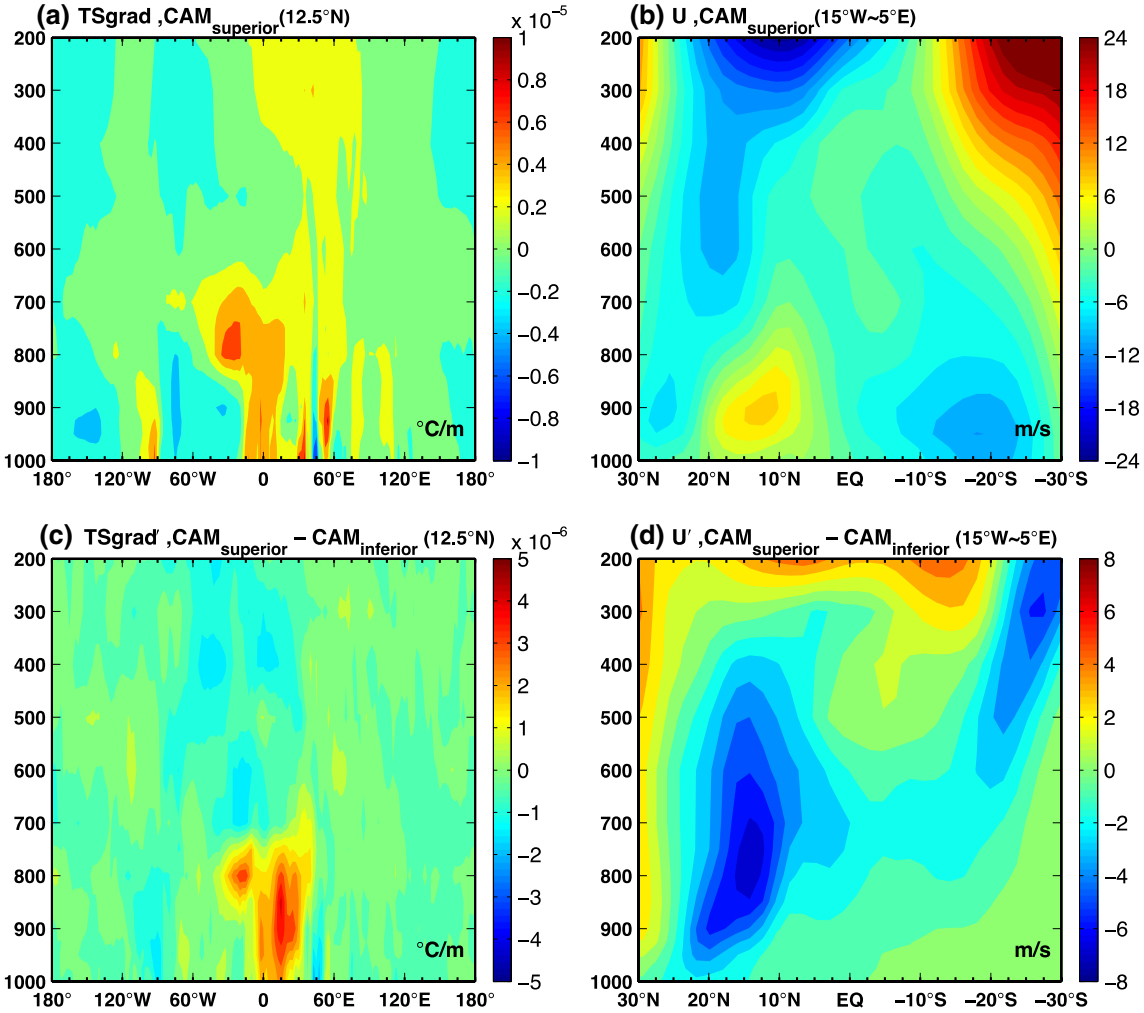

Fig. 11 Vertical cross section of the meridional temperature gradient at 12.5°N in August 2000 for **a** the superior group and **c** the difference between the superior and inferior groups. The vertical cross section of the mean zonal wind over West Africa (15°W–5°E) in August 2000 for **b** the superior group and **d** the difference between the superior and inferior groups

intercomparison of Xue et al. (2010b), which found that the evolution of the WAM precipitation is closely related to the enhanced Sahara mode (i.e., SHL discussed in our study) and the weakened Sahel mode. Our results further show that, even using the same CAM3.5/CLM3.5 with the same surface boundary condition, the model uncertainty resulting only from the breeding of atmospheric instability can be large enough to trigger the significant change of jet strength and SHL location, nevertheless the long-term integration in the CMIP3 and CMIP5 models. Without serious consideration of the internal variability within the model dynamics, any conclusions about the future projection of the Sahel rainfall should be made with caution.

It has been well-known that these atmospheric jet dynamics may alter the location and amplitude of the SHL at all scales (Ramel et al. 2006) and may thus be linked to the location of convergence at low levels (Biasutti et al. 2009). Our diagnostics show that these characteristics are the key to reduce the individual model uncertainty and can explain a large portion of the discrepancy in our short-range ensemble hindcasts of precipitation. Ocean variability or anthropogenic forcing is not the only factor modulating rainfall variability in the Sahel according to our short-range ensemble hindcasts which have unchanged surface boundary conditions. Rather, the key factor is the coupling between the circulation associated with the SHL and the ascent associated with the tropical rainbelt (divergence/convergence). Tomas and Webster (1997) suggested that the AWJ results not only from the WAM but also from an inertial instability mechanism because of a cross-equatorial pressure gradient from the South Atlantic High that leads to off-equatorial convection in the lower

level. This may have caused the modeled precipitation bias and the large uncertainty in this sensitive region since the dynamical perturbation can easily trigger the evident differences between the superior (reducing errors) and inferior (enhancing errors) groups by the growth of instability errors (Cook 2015). Then, the land–atmosphere feedback and its coupling with the atmosphere may further influence precipitation patterns in this region (Entekhabi 1995; Cook 1999; Koster et al. 2004; Xue et al. 2010a) through changes in the SHL and AEJ. Comparing the differences in the superior and inferior groups indicated that the soil moisture and low-level BL temperature gradients may affect the location and magnitude of the AEJ, creating a favorable environment for jet instabilities to develop (Cook 1999, 2015). The model instability is likely the driving forcing that triggers large variances in the AEJ and the associated SHL dynamics, initiated from the low-level BL. The critical region to enhance the atmospheric instability may be that between the SHL and the tropical rainbelt (the largest difference in Fig. 5).

In addition, our diagnosis indicated that changes in the SHL location and amplitude associated with changes in the AEJ may result from changes in the low-level BL temperature gradient. As a consequence, the modeled atmospheric divergence as a result of the different AEJ and TEJ greatly affect the modeled precipitation and temperature. The local land–atmosphere feedback may also enhance the temperature growth through the dynamical perturbations every 6-hourly even though the perturbations are small. The model uncertainty grows quickly in time due to the growth of the instability, triggered by the perturbations. Thus, the interactions among the WAM, ITCZ convection, and atmospheric jet dynamics change the modeled Sahel precipitation patterns. Local atmospheric jets have a more direct impact than does remote oceanic forcing, confirming the controlling role of the SHL in the disagreement of MMEs (Biasutti et al. 2009) and the model bias in the other models (e.g., Vellinga et al. 2013; Diallo et al. 2014). Further refinement of the model dynamics is required to minimize the biases associated with the SHL and AEJ in order to settle future climate projection disagreements.

MMEs have commonly been used in climate projections (e.g., IPCC 2007, 2013; Roehrig et al. 2013) and are powerful tools to account for structural uncertainties (either numerical or physical) arising from specific model errors in dynamic model-based predictions. The MMEs provide good estimates of model errors in terms of the ensemble model spread. However, MMEs may yield probabilistic risk forecasts of climate events (Palmer et al. 2005), particularly in some sensitive regions where the model uncertainty is large. Any structural uncertainty or model bias (i.e., errors introduced by the model design) is difficult to control when the spread of MMEs is too broad (e.g., Sahel precipitation in the climate model projections shown in IPCC 2007, 2013). Estimating the built-in structural uncertainties of Sahel precipitation for each model is almost impossible in the CMIP3 and CMIP5 climate models because substantial contradictions exist in signs of future precipitation changes; some models are locked in a persistently dry scenario, whereas others predict the opposite.

The short-range ensemble hindcasts used here can minimize the structural uncertainty inherent in individual models because of the constraints of meteorological fields and the enhanced growth of physical instability (Yang et al. 2006). Therefore, the system can reduce and control uncertainties more effectively than MMEs do (e.g., only noticeable biases and large spreads in the Sahel region in Fig. 2). These ensembles provide an alternative to determining and quantifying model biases by constraining large ensembles using the observations. Our results confirmed the well-captured influence of the Atlantic on rainfall in the West Sahel (very small uncertainty among the ensembles). A major source of systematic biases results from the erroneous location and magnitude of SHL and AEJ, where the relevant processes are likely amplified by land–atmosphere feedback and initiated from the low-level BL temperature gradient. A large spread of precipitation and temperature was observed in the ensembles within a few months despite the small spread in the initial atmospheric perturbations (approximately 5–10 % in the Sahel, not shown here). This was expected because subsequent rainbelt development was independent of the perturbations, and the precipitation and surface temperature were not assimilated in the system. This is a fast process dynamic within a few months so that the model biases occur quickly without long-integration of the climate model. The accuracy of precipitation is heavily determined by model physics and dynamics. The current approach assisted us in determining the model dynamics and physics responsible for the bias and in quantifying uncertainty.

7 Conclusion

The data-assimilated short-range ensemble hindcast system was introduced to diagnose the Sahel precipitation based on the CAM3.5/CLM3.5 climate model. Using a single model with identical surface boundary condition, the ensemble hindcasts effectively detected a source of structural uncertainties causing the Sahel precipitation and temperature biases within a few months. No long-term integration is required to isolate this bias in the global CAM3.5/CLM3.5. This approach is different from the commonly used SST/land forcing sensitivity model studies in that we can effectively detect the uncertainties only related to dynamical or thermodynamic instability mechanism within

a short time. The SST/land forcing sensitivity experiments may potentially trigger not only the instability mechanism discussed here, but also the other mechanisms which may complicate the analysis. The model uncertainties generated by the instability emphasized in this paper need to be significantly reduced for any credential sensitivity study. Since we identify the biases are initiated from the low-level BL temperature gradient on land, an improved atmospheric BL model is likely required to minimize the model's systematic biases.

This approach is also different from the MMEs and other ensemble experiments. The built-in structural uncertainties may be even larger in the MMEs, potentially introducing larger model diversity. In MMEs and other ensemble experiments, the mean and variance of climate sensitivity are commonly used to produce a probability-density function and analyze the uncertainty, which depends heavily on the choice of realization. However, it is difficult to determine the cause of biases in MMEs if the ensemble spreads are too broad with large uncertainty in the region of interest. By comparing the superior and inferior groups (corresponding to the different growth of errors), we demonstrate that the proposed ensemble hindcasts provide a useful diagnosis of model biases, specifically for biases closely related to the physical instability, based on quantitative measures of similarity with observations; it can potentially be used to obtain better weighted ensemble members, which may effectively reduce the model-data discrepancy in future climate projections.

The ensemble mean of the CAM3.5/CLM3.5 hindcasts did not provide accurate precipitation and temperature predictions that were similar to observations. Further diagnosis of the ensembles showed that the precipitation and temperature biases resulted directly from atmospheric jet dynamics (such as the AWJ, AEJ, and TEJ) and associated wave disturbance triggered by the model instability in the atmospheric BL on land. In addition, amplification by land–atmosphere feedback was not negligible. Comparison with observations confirmed that the SHL and AEJ play an essential role in rainfall changes in the Sahel, particularly in central to northeast Africa, and might be the major cause of the inconsistency in the hindcast experiment. Further understanding of these mechanisms in the model dynamics to minimize the biases can significantly improve model prediction and climate projection.

We also found the influence of remote ocean variability and the land–sea thermal contrast did not control these characteristics since all surface boundary conditions were unchanged in the model ensembles. However, such processes might affect internal variability in the model dynamics in the long-term integration at the interannual to decadal scales; this requires further investigation next with caution. The overall warming of the ocean might further enhance oceanic evaporation and, thus, fuel convection and rainfall over water at the expense of continental convection (Chou and Neelin 2004). We identified the location and magnitude of the SHL and AEJ controlled a major bias of precipitation and temperature patterns, resulting from local divergence and convergence. This accounts for approximately 25 % of precipitation and 16 % of temperature biases in the model. Our study can provide a crucial guideline for modeling the Sahel rainfall variability in the future. Without serious consideration of the location and magnitude of the SHL and the AEJ within the model's internal variability, any conclusions about the future projection of the Sahel drought should be made with caution.

Acknowledgments Constructive comments and suggestions from the three anonymous reviewers are really appreciated. The author would also like to thank Dr. Junjie Liu for providing the ensemble model configurations and Prof. Inez Fung for the initialization of this project. The author acknowledges the computing resource of NERSC, Lawrence Berkeley National Laboratory, USA and National Center for High Performance Computing, Taiwan. The Climate Research Unit (CRU) TS3.1 dataset is available online at http://www.cru.uea.ac.uk/data. NCAR is sponsored by the U. S. National Science Foundation (NSF). Y. H. Tseng was partially supported by the NSF Earth System Model (EaSM) Grant 1419292 (EaSM-3: Collaborative Research: Quantifying Predictability Limits, Uncertainties, Mechanisms, and Reagional Impacts of Pacific Decadal Climate Variability). Y.-H. Lin and M.-H. Lo were supported by the Ministry of Science and Technology, Taiwan (Grant of MOST 103-2111-M-002-006).

References

Adler RF, Huffman GJ, Chang A, Ferraro R, Xie P, Janowiak J, Rudolf B, Schneider U, Curtis S, Bolvin D, Gruber A, Susskind J, Arkin P (2003) The version 2 Global Precipitation Climatology Project (GPCP) monthly precipitation analysis (1979–Present). J Hydrometeor 4:1147–1167

Biasutti M, Sobel AH, Camargo SJ (2009) The role of the SHL in summertime Sahel rainfall variability and change in the CMIP3 models. J Clim 22:5755–5771

Bowler NE (2006) Comparison of error breeding singular vectors, random perturbations and ensemble Kalman filter perturbation strategies on a simple model. Tellus A 58:538–548

Buehner M, Mahidjiba A (2010) Sensitivity of global ensemble forecasts to the initial ensemble mean and perturbations: comparison of EnKF, singular vector, and 4D-Var approaches. Mon Wea Rev 138:3886–3904

Buizza R, Gelaro R, Molteni F, Palmer TN (1997) The impact of increased resolution on predictability studies with singular vectors. Q J R Meteorol Soc 123:1007–1033

Burpee RW (1972) The origin and structure of easterly waves in the lower troposphere of North Africa. J Atmos Sci 29:77–90

Chang C-Y, Chiang JCH, Wehner MF, Friedman A, Ruedy R (2011) Sulfate aerosol control of tropical Atlantic climate over the 20th century. J Clim 24:2540–2555

Charney J (1975) Dynamics of deserts and drought in the Sahel. Q J R Meteor Soc 101:193–202

Chou C, Neelin JD (2004) Mechanisms of global warming impacts on regional tropical precipitation. J Clim 17:2688–2701

Cook KH (1999) Generation of the African Easterly jet and its role in determining West African precipitation. J Clim 12:1165–1184

Cook KH (2008) The mysteries of Sahel droughts. Nat Geosci 1:647–648

Cook KH (2015) Role of inertial instability in the West African monsoon jump. J Geophys Res Atmos 120:3085–3102
Cook KH, Vizy EK (2006) Coupled model simulations of the West African monsoon system: 20th century simulations and 21st century predictions. J Clim 19:3681–3703
Corazza M, Kalnay E, Patil DJ, Yang S-C, Hunt B, Szunyogh I, Yorke J (2003) Relationship between bred vectors and the errors of the day. Nonlinear Proc Geophys 10:233–243
Dai A, Lamb PJ, Trenberth KE, Hulme M, Jones PD, Xie P (2004) The recent Sahel drought is real. Int J Climatol 24:1323–1331
Diallo I, Sylla MB, Camara M, Gaye AT (2013) Interannual variability of rainfall over the Sahel based on multiple regional climate models simulations. Theor Appl Climatol 113:351–362
Diallo I, Bain CL, Gaye AT, Moufouma-Okia W, Niang C, Dieng MDB, Graham R (2014) Simulation of the West African monsoon onset using the HadGEM3-RA regional climate model. Clim Dyn 43:575–594
Doherty R, Kutzbach JE, Foley JA, Pollard D (2000) Fully coupled climate/dynamical vegetation model simulations over northern Africa during the mid-Holocene. Clim Dyn 16:561–573
Douville H, Salas-Mélia D, Tyteca S (2006) On the tropical origin of uncertainties in the global land precipitation response to global warming. Clim Dyn 26:367–385
Eltahir EAB (1998) A soil moisture–rainfall feedback mechanism: 1. Theory and observations. Water Resour Res 34:765–776
Entekhabi D (1995) Recent advances in land–atmosphere interaction research. Rev Geophys 33:995–1003
Entekhabi D, Rodriguez-Iturbe I (1994) An analytic framework for the characterization of the spacetime variability of soil moisture. Adv Water Resour 17:25–45
Feng J, Ding R, Liu D, Li J (2014) The Application of nonlinear local Lyapunov vectors to ensemble predictions in Lorenz systems. J Atmos Sci 71:3554–3567
Feng L, Zheng F, Zhu J, Liu H (2015) The role of stochastic model error perturbations in predicting the 2011/12 double-dip La Niña. SOLA 11:65–69
Folland CK, Palmer TN, Parker DE (1986) Sahel rainfall and worldwide sea temperatures, 1901–85. Nature 320:602–607
Gent PR, Yeager SG, Neale RB, Levis S, Bailey DA (2010) Improvements in a half degree atmosphere/land version of the CCSM. Clim Dyn 34:819–833
Giannini A, Biasutti M, Verstraete MM (2008) A climate model-based review of drought in the Sahel: desertification, the re-greening and climate change. Glob Planet Change 64:119–128
Held IM, Delworth TL, Lu J, Findell K, Knutson TR (2005) Simulation of Sahel drought in the 20th and 21st centuries. Proc Natl Acad Sci 102:17891–17896
Hoerling MP, Hurrell JW, Eischeid J, Phillips A (2006) Detection and attribution of 20th century Northern and Southern African rainfall change. J Clim 19:3989–4008
Hoffman MJ, Kalnay E, Carton JA, Yang S-C (2009) Use of breeding to detect and explain instabilities in the global ocean. Geophys Res Lett 36:L12608. doi:10.1029/2009GL037729
Hunt BR, Kostelich EJ, Szunyogh I (2007) Efficient data assimilation for spatiotemporal chaos: a local ensemble transform Kalman filter. Phys D 230:112–126
Hurrell JW, Hack JJ, Shea D, Caron JM, Rosinski J (2008) A new sea surface temperature and sea ice boundary dataset for the Community Atmosphere Model. J Clim 21:5145–5153
IPCC (2007) Climate change 2007: the physical science basis. In: Solomon S, Qin D, Manning M, Chen Z, Marquis M, Averyt KB, Tignor M, Miller HL (eds) Contribution of working group I to the fourth assessment report of the intergovernmental panel on climate change. Cambridge University Press, Cambridge, p 996
IPCC (2013) Climate Change 2013: the physical science basis. In: Stocker TF, Qin D, Plattner G-K, Tignor M, Allen SK, Boschung J, Nauels A, Xia Y, Bex V, Midgley PM (eds) Contribution of working group I to the fifth assessment report of the intergovernmental panel on climate change. Cambridge University Press, Cambridge, p 1535
James R, Washington R, Rowell DP (2014) African climate change uncertainty in perturbed physics ensembles: implications of global warming to 4°C and beyond. J Clim 27:4677–4692
Janicot S, Gaetani M, Hourdin F, Giannini A, Biasutti M, Mohino E, Xue Y, Boone A, Gaye A, Salack S, Lavaysse C (2015) The recent partial recovery in Sahel rainfall: a fingerprint of greenhouse gases forcing? GEWEX News 27:11–15
Kalnay E, Toth Z (1994) Removing growing errors in the analysis cycle. In: Tenth conference on numerical weather prediction, pp 212–215
Kanamitsu M, Ebisuzaki W, Woollen J, Yang SK, Hnilo JJ, Fiorino M, Potter GL (2002) NCEP-DOE AMIP-II Reanalysis (R-2). Bull Am Meteor Soc 83:1631–1643
Knippers P (2003) Tropical-extratropical interactions causing precipitation in Northwest Africa: statistical analysis and seasonal variations. Mon Wea Rev 131:3069–3076
Koster RD et al (2004) Regions of strong coupling between soil moisture and precipitation. Science 305:1138–1140
Lebel T, Didhiou A, Laurent H (2003) Seasonal cycle and interannual variability of the Sahelian rainfall at hydrological scales. J Geophys Res 108:8389
Liu J, Chahine MT, Kalnay E, Fung I, Olsen ET (2009) Assimilation of AIRS and conventional CO2 observations with an EnKF. Eos Trans AGU 90, Fall Meet. Suppl., Abstract A51A-0086
Liu J, Fung I, Kalnay E, Kang J-S (2011) CO2 transport uncertainties from the uncertainties in meteorological fields. Geophys Res Lett 38:L12808. doi:10.1029/2011GL047213
Liu J, Fung I, Kalnay E, Kang J-S, Olsen ET, Chen L (2012) Simultaneous assimilation of AIRS Xco2 and meteorological observations in a carbon climate model with an ensemble Kalman filter. J Geophys Res 117:D05309. doi:10.1029/2011JD016642
Lo M-H, Famiglietti JS (2011) Precipitation response to land subsurface hydrologic processes in atmospheric general circulation model simulations. J Geophys Res 116:D05107. doi:10.1029/2010JD015134
Magnusson L, Leutbecher M, Källén E (2008) Comparison between singular vectors and breeding vectors as initial perturbations for the ECMWF ensemble prediction system. Mon Wea Rev 136:4092–4104
Matthews AJ (2004) Intraseasonal variability over tropical Africa during northern summer. J Clim 17:2427–2440
Neale RB, Richter JH, Jochum M (2008) The impact of convection on ENSO: from a delayed oscillator to a series of events. J Clim 21:5904–5924
Neelin JD, Chou C, Su H (2003) Tropical drought regions in global warming and El Niño teleconnections. Geophys Res Lett 30:2275. doi:10.1029/2003GL018625
Nicholson SE (2009) A revised picture of the structure of the "monsoon" and land ITCZ over West Africa. Clim Dyn 32:1155–1171
Nicholson SE (2013) The west African Sahel: a review of recent studies on the rainfall regime and its interannual variability. ISRN Meteorol. doi:10.1155/2013/453521
Nicholson SE, Palao IM (1993) A re-evaluation of rainfall variability in the Sahel. Part I. Characteristics of rainfall fluctuations. Int J Climatol 13:371–389
Nicholson SE, Webster PJ (2007) A physical basis for the interannual variability of rainfall in the Sahel. Quart J R Meteor Soc 133:2065–2084
Oleson KW, Niu GY, Yang ZL (2008) Improvements to the Community Land Model and their impact on the hydrological cycle. J Geophys Res 113:G01021

Palmer T, Doblas-Reyes F, Hagedorn R, Weisheimer A (2005) Probabilistic prediction of climate using multi-model ensembles: from basics to applications. Philos Trans R Soc Lond B Biol Sci 360:1991–1998

Qian C, Zhang F, Green BW, Zhang J, Zhou X (2013) Probabilistic evaluation of the dynamics and prediction of supertyphoon Megi (2010). Wea Forecasting 28:1562–1577

Ramel R, Gallée H, Messager C (2006) On the northward shift of the West African monsoon. Clim Dyn 26:429–440

Richter JH, Rasch PJ (2008) Effects of convective momentum transport on the atmospheric circulation in the Community Atmosphere Model, version 3. J Clim 21:1487–1499

Rodríguez-Fonseca B et al (2015) Variability and predictability of west African droughts: a review on the role of sea surface temperature anomalies. J Clim 28:4034–4060

Roehrig R, Bouniol D, Guichard F, Hourdin F, Redelsperger J-L (2013) The present and future of the west African monsoon: a process-oriented assessment of CMIP5 simulations along the AMMA Transect. J Clim 26:6471–6505

Stockli R, Lawrence DM, Niu G-Y, Oleson KW, Thornton PE, Yang Z-L, Bonan GB, Denning AS, Running SW (2008) Use of FLUXNET in the Community Land Model development. J Geophys Res 113:G01025

Tomas R, Webster PJ (1997) On the location of the intertropical convergence zone and near-equatorial convection: the role of inertial instability. Q J R Met Soc 123:1445–1482

Toth Z, Kalnay E (1993) Ensemble forecasting at NMC: the generation of perturbations. Bull Am Meteor Soc 74:2317–2330

Toth Z, Kalnay E (1997) Ensemble forecasting at NCEP and the breeding method. Mon Wea Rev 125:3297–3319

Vellinga M, Arribas A, Graham R (2013) Seasonal forecasts for regional onset of the West African monsoon. Clim Dyn 40:3047–3070

Wang C, Dong S, Evan AT, Foltz GR, Lee S-K (2012) Multidecadal covariability of North Atlantic sea surface temperature, African dust, Sahel rainfall, and Atlantic hurricanes. J Clim 25:5404–5415

Wei M, Toth Z, Wobus R, Zhu Y (2008) Initial perturbations based on the ensemble transform (ET) technique in the NCEP global operational forecast system. Tellus A 60:62–79

Xie P, Arkin PA (1996) Analyses of global monthly precipitation using gauge observations, satellite estimates, and numerical model predictions. J Clim 9:840–858

Xue Y, Shukla J (1993) The influence of land surface properties on Sahel climate. Part I: desertification. J Clim 6:2232–2245

Xue Y, Liou KN, Kasahara A (1990) Investigation of biogeophysical feedback on the African climate using a two-dimensional model. J Clim 3:337–352

Xue Y, De Sales F, Vasic R, Mechoso CR, Arakawa A, Prince S (2010a) Global and seasonal assessment of interactions between climate and vegetation biophysical processes: a GCM study with different land–vegetation representations. J Clim 23:1411–1433

Xue Y et al (2010b) Intercomparison and analyses of the climatology of the west African monsoon in the west African monsoon modeling and evaluation project (WAMME) first model intercomparison experiment. Clim Dyn 35:3–27

Yang S-C, Cai M, Kalnay E, Rienecker M, Yuan G, Toth Z (2006) ENSO bred vectors in coupled ocean-atmosphere general circulation models. J Clim 19:1422–1436

Zhang F (2005) Dynamics and structure of mesoscale error covariance of a winter cyclone estimated through short-range ensemble forecasts. Mon Wea Rev 133:2876–2893

Zhang R, Delworth T (2006) Impact of Atlantic multidecadal oscillations on India/Sahel rainfall and Atlantic hurricanes. Geophys Res Lett 33:L17712. doi:10.1029/2006GL026267